Supplementary material

Modeling of Gas-Wall Partitioning of Organic Compounds Using a Quantitative Structure-Activity Relationship

Sanghee Han, Myoseon Jang*, and Huanhuan Jiang

Department of Environmental Engineering Science, University of Florida, Gainesville, Florida, USA

Correspondence to: Myoseon Jang (mjang@ufl.edu)

This file includes:
Figures S1~S5
Tables S1~S5
References

Section S1 Outdoor chamber experiments

Outdoor chamber operation

The Atmospheric PHotochemical Outdoor Reactor (UF-APHOR) dual chambers are located on the rooftop of Black Hall (29˚38'31" N, 82˚20'52" W) at the University of Florida, Gainesville, Florida. UF-APHOR is made with Fluorinated Ethylene Propylene (FEP) Teflon film. For the study of the Gas-Wall Process (GWP) of a Semivolatile Organic Compound (SVOC), a cocktail of 21 SVOCs was injected into the UF-APHOR using a glass manifold under a clean air stream at night. The time required for the chemical injection can delay measurement of the SVOCs' gaseous concentrations. To reduce the delay, the injection of organic compounds was performed in two steps (Fig. S1). First, organic compounds were injected into the East chamber (door between the two chambers closed). Second, the organic vapor in the East chamber was transferred to the West chamber quickly by opening the door between the two chambers and circulating the air using a small desk fan and a slow mixing (rpm=60) fan for 10 minutes. Then, SVOC gas collection began using a 40-cm 5-channel annular denuder coated with XAD-4 resin powder. The experiment was conducted for 6 hours. CCl_4 (>99.9%, Sigma Aldrich, St. Louis, MO, USA) was injected into the chamber to monitor the chamber dilution using Gas Chromatography with a Frame Ionization Detector (GC-FID, Hewlett-Packard 5890, Palo Alto, CA, USA). The SVOC vapor was collected for 15 minutes in 10-minute intervals from the beginning of the experiment. After 1.2 h, the sampling interval (0.5 to 1 h) and duration (30 to 40 min) were increased.

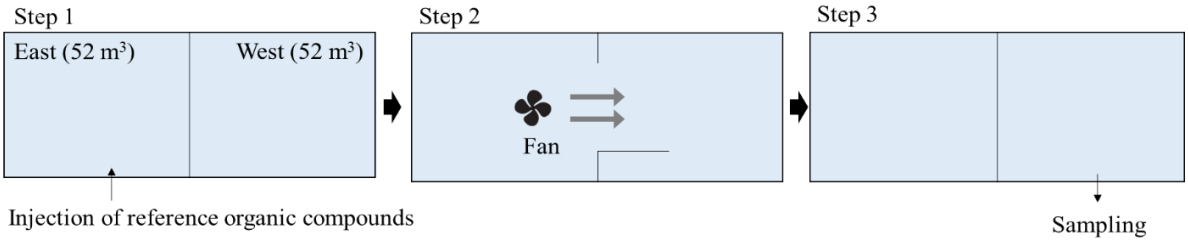

Figure S1. The experimental procedure from chemical injection to sampling.

Measurement of SVOC vapor concentrations using GC/MS

A 20 µL internal standard stock solution with 6 deuterated polycyclic aromatic hydrocarbons (23.68 mg mL^{-1} naphthalene-d_8 (>98%, Aldrich, St. Louis, MO, USA), 30.86 mg mL^{-1} acenaphthylene-d_{10} (neat, Aldrich, St. Louis, MO, USA), 26.66 mg mL^{-1} anthracene-d_{10} (neat, Aldrich, St. Louis, MO, USA), 34.32 mg mL^{-1} fluoranthene-d_{10} (neat,

Aldrich, St. Louis, MO, USA), 35.84 mg mL^{-1} pyrene-d_{10} (98%, Aldrich, St. Louis, MO, USA), and 20.74 mg mL^{-1} chrysene-d_{12} (neat, Aldrich, St. Louis, MO, USA)) was spiked to the XAD-coated denuder after sampling. The sample was extracted by filling with 50 mL dichloromethane (99.9%, Fisher Pittsburgh, PA, USA) and inverting 20 times. This process was repeated three times. The extracted sample was concentrated by blowing the solvent down to ~6 mL with rotary evaporation (Heidolph Rotary Evaporator Laborota 4001, Schwabach, Germany) at 80 ºC and farther to ~0.7 mL using a six-port evaporator (Sigma-Aldrich, St. Louis, MO, USA). Th magnesium sulfate powders (50 mg) were added to the concentrated extracts to remove the water, after which the samples were split into two GC vials. One was applied directly to the gas chromatography/mass spectrometer (GC/MS) (Varian 3800/2000 GC/MS, Palo Alto, CA, USA) analysis. The alcohols and carboxylic acids in this vial were derivatized by adding 1 µL N,O-bis(trimethylsilyl)trifluoroacetamide (BSTFA) (0.192 g mL^{-1}) and were incubated for 30 min at 40 °C.

A 2 µL denuder-extracted sample was injected in the on-column mode to GC/MS. The column oven temperature was held at 65 °C for 0.5 min, and then ramped to 100 °C at a 15 °C min^{-1} gradient and held for 2.5 min, and ramped finally to 280 °C at a 12 °C min^{-1} gradient and held for 8 min. The individual compounds in the particle extracts were identified using an external standard and analyzed tentatively using the National Institute of Standards and Technology (NIST) library.

SVOCs for the study of GWP

1-heptanoic acid (98%), Phenol (99%, extra pure), dimethoxyphenol (99%, extra pure), 2,6-dimethylphenol (99%, extra pure), 1-octanol (99%), and 2-dodecanone (95%) were obtained from ACROS organics (NJ, USA). Pyruvic acid (98%), 1-hexanoic acid (99.5%), 1-octanoic acid (>99%, extra pure), 2-heptanol (98%), 1-nonanol (98%), citral (95%), and benzaldehyde (>99%, extra pure) were obtained from Sigma-Aldrich (St. Louis, MO, USA). D42-eicosane (98%) and D40-nonadecane (98%) were obtained from Cambridge Isotope Laboratories, Inc. (Tewksbury, MA, USA). n-heptadecane (99%) and 2-tridecanone (>98%) were obtained from Alfa Aesar (HaverHill, MA, USA). Benzoic acid (99%) and benzyl alcohol (>99%) were obtained from Fisher Scientific (Pittsburgh, PA, USA).

Section S2. Absorbing organic matter (OM_{wall}) and hygroscopicity of OM_{wall}

Chemical composition of organic composition of OM_{wall} ($M_{wall-OM}$)

In Fig. S2, the two different FTIR spectra obtained in different time shows the similar compositions, suggesting that the organic composition of OM_{wall} ($M_{wall-OM}$) can be fixed in a certain functional composition.

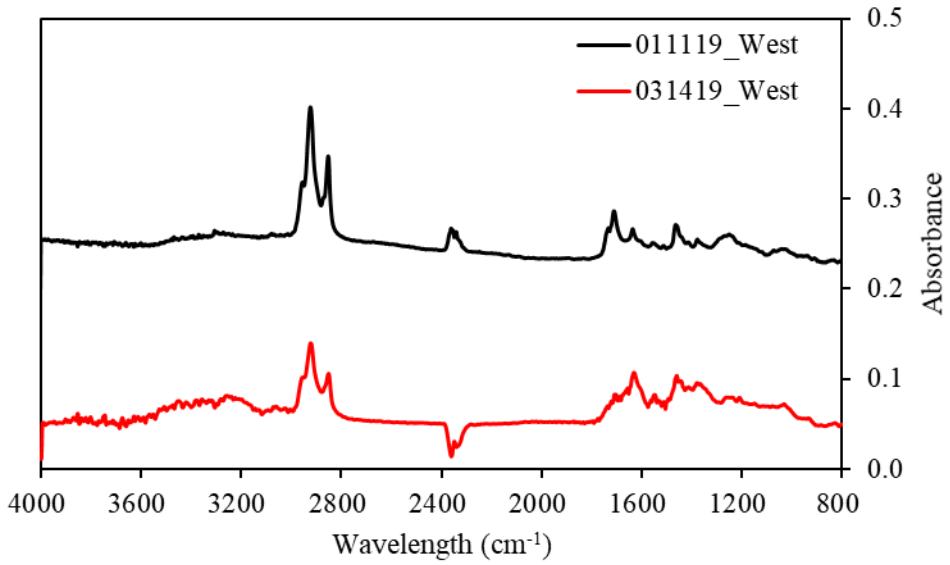

Figure S2. FTIR spectrum of extracted OM_{wall} from two different part of inside chamber on different date. FTIR spectrum is normalized by concentration of OM_{wall} (011119_West: 6.62 mg m^{-3} and 031419_West: 5.40 mg m^{-3}).

OM_{wall} was collected by wiping the wall (400 cm^2) with a nylon filter and 10 mL acetone (HPLC 99.7%, Fisher Science, Pittsburgh, PA, USA). The composition of $M_{wall-OM}$'s functional groups was determined using a Fourier transform Infrared Spectrum (FTIR) (Nicolet Magma 560, Madison, WI, USA). The OM_{wall} extracted was concentrated using dry air from a dry air tank (Breathing air, Air gas). The OM_{wall} solution was concentrated further on the FTIR silicone disk (13 × 2 mm, Sigma–Aldrich, St Louis, MO, USA).

Table S1. Summarized composition of $M_{wall-OM}$ by fitting FTIR spectrum of extracted OM_{wall} with pure compounds following a curve- filling method of Li et al. (2016).

Functionalities	-CH	-OH	-COOH	C=O	C=C
Relative composition	1	0.086	0.043	0.024	0.083

Hygroscopicity of OM_{wall}

The hygroscopicity of solvent extracted OM_{wall} was determined using an FTIR spectrometer (Nicolet Magma 560, Madison, WI, USA) interfaced with a specifically fabricated optical flow chamber by controlling the relative humidity in the range from 0.1 to 0.8. Humidity was controlled by combining humid air from a water bubbler and dry air from a dry air tank (Jang et al., 2010; Beardsley et al., 2013; Zhong and Jang, 2014). Calibration curves for water content ($M_{wall\text{-}water}$, mg m^{-3}) of OM_{wall} were obtained by the same method as Jang et al. (2010). The FTIR absorbance of the water peak ($Abs_{water,}$ 3350 cm^{-1}) at different RH and the water mass fraction predicted from an inorganic thermodynamic model were related to determine the calibration curve. The water content estimated with the calibration curve was converted to the $M_{wall\text{-}water}$ of this study with the volume, surface area of the chamber, and the surface area of the Teflon film (0.4 m^2) used to extract OM_{wall}. Fig. S3 illustrates hygroscopicity of OM_{wall}.

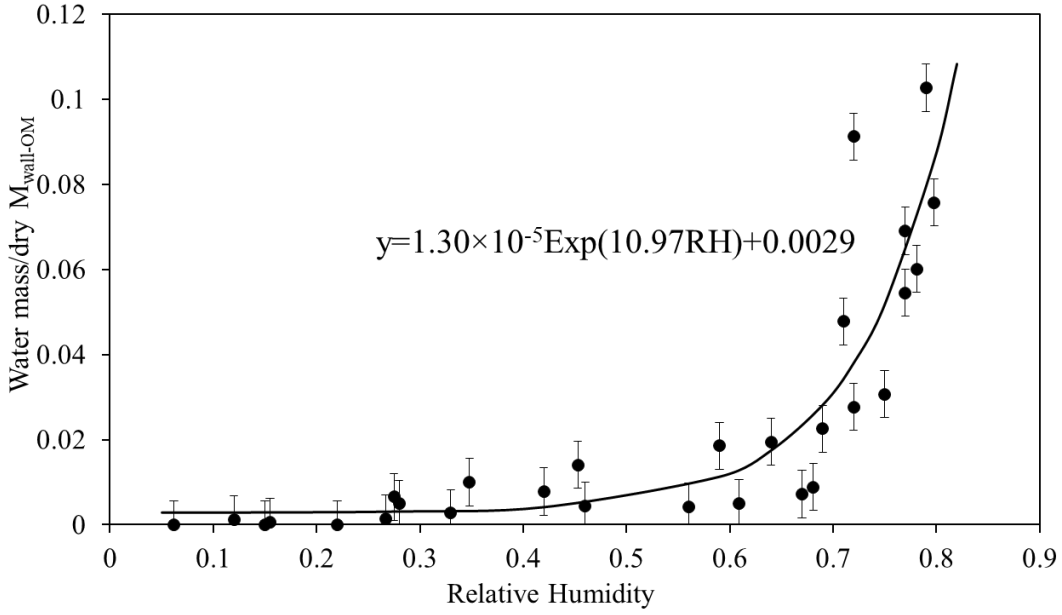

Figure S3. The water content of extracted $M_{wall\text{-}OM}$ from the surface of the FEP Teflon film (20 cm x 20 cm) was measured using the FTIR spectrometer interfaced with the specially designed flow tube to control relative humidity between 0.05 to 0.80. The Teflon film's surface area (0.4 m^2), the UF-APHOR chamber's surface area (86 m^2), and volume (52 m^2) were applied as parameters to obtain the water content of the dry organic matter. The error bar associated with the water mass was estimated with the uncertainty in FTIR absorbance and aerosol mass.

Mass concentration of $M_{wall\text{-}OM}$ and its molecualr weight

$M_{wall\text{-}OM}$ was measured in two different ways; extracted from the Teflon film with organic solvent and extracted from the chamber inside by wiping the wall with acetone. The Teflon film was extracted with organic solvents (acetone and dichloromethane) and the mass was obtained from the difference in mass before and after extraction. $M_{wall\text{-}OM}$ mass was fit at 18.52 mg m^{-3}, which was obtained by averaging the mass of extracted $M_{wall\text{-}OM}$ measured (11.81 mg m^{-3} and 25.22 mg m^{-3}). $M_{wall\text{-}OM}$ was collected by wiping the Teflon film over the surface area (20 cm × 20 cm) with an acetone-drenched nylon filter. Extracted OM_{wall} was concentrated onto a FTIR silicone disk using clean air and the mass was obtained from the difference weight of before and after placing the sample on the FTIR disc using an analytical balance (Mettler Toledo MX5 microbalance, Columbus, OH, USA). The $M_{wall\text{-}OM}$ mass (6.9 mg m^{-3}) extracted via wiping the Teflon film may be biased negatively because the wiping method can be imperfect. Thus, the $M_{wall\text{-}OM}$ used in this study was set at 18.52 mg m^{-3}. The molecular weight of OM_{wall} (MW_{OM}) was estimated theoretically using the group contribution method (Barton, 1991; Jang et al., 1997; Jang and Kamens, 1998) by optimizing MW_{OM} until the activity of liquid water in OM_{wall} equaled the humidity at the given chemical composition of $M_{wall\text{-}OM}$ (FTIR data). At a given $M_{wall\text{-}OM}$ (18.52 mg m^{-3}), estimated MW_{OM} was 273.3 g mol^{-1}.

Section S3. Statistical analyses of the QSAR-based model to predict $K_{w,i}$ and $\alpha_{w,i}$

To model the impact of RH on $K_{w,i}$, the polynomial equation correlated to QSAR parameters was derived for the three datasets obtained under the three different humidity levels. If the descriptors are constructed carefully, the model can be applied to predict various organic compounds' $K_{w,i}$ and $\alpha_{w,i}$ that are not included in the initial dataset. Table S2 summarizes the resulting linear regression coefficients for each experiment. The p-value of parameter E_i in two datasets (RH =0.75 and 0.001) was insignificant (p-value > 0.05). Thus, parameter E_i was eliminated from the polynomial equation. Except for parameter $H_{a,i}$, other parameters' significance varied with the dataset. Based on the p-values, R^2 and adjusted R^2 values in linear regressions, parameters $H_{d,i}$, $H_{a,i}$, α_i, and S_i were applied to the derivation of the QSAR-based polynomial equation. Fig. S4 illustrates the linear relation between $\ln(\gamma_{w,i})$ with each coefficient of physicochemical paramters.

Table S2. The statistical procedure and results for the QSAR-based polynomial model equation used to predict ln($\gamma_{w,i}$) at the three different humidity levels.

RH=0.40 (Oct 8, 2018)						
Descriptor	$H_{d,i}$	$H_{a,i}$	α_i	S_i	E_i	R^2 (Adj-R^2)
Coefficients	4.24	-0.42	0.20	1.07	1.12	0.99 (0.91)
P-value	2.5×10^{-7}	5.0×10^{-1}	1.3×10^{-14}	4.0×10^{-2}	3.6×10^{-2}	
Coefficients	3.68	1.61	0.20	0.017		0.99 (0.91)
P-value	1.8×10^{-4}	3.8×10^{-1}	3.6×10^{-11}	9.0×10^{-1}		
Coefficients	3.68	1.65	0.20			0.99 (0.91)
P-value	9.7×10^{-4}	1.6×10^{-1}	5.1×10^{-12}			
RH=0.72 (May 15, 2018)						
Descriptor	$H_{d,i}$	$H_{a,i}$	α_i	S_i	E_i	R^2 (Adj-R^2)
Coefficients	3.27	-0.89	0.19	-0.16	0.79	0.99 (0.88)
P-value	1.7×10^{-7}	8.0×10^{-1}	4.2×10^{-9}	8.9×10^{-1}	5.0×10^{-1}	
Coefficients	3.09	0.90	0.20	0.4		0.99 (0.89)
P-value	5.2×10^{-2}	7.2×10^{-1}	4.0×10^{-10}	5.7×10^{-1}		
Coefficients	2.79	1.98	1.98			0.99 (0.89)
P-value	4.8×10^{-2}	2.3×10^{-1}	6.1×10^{-11}			
RH<0.001 (literature data[a])						
Descriptor	$H_{d,i}$	$H_{a,i}$	α_i	S_i	E_i	R^2 (Adj-R^2)
Coefficients	5.64	5.85	0.19	2.43	5.45	0.99 (0.93)
P-value	2.0×10^{-2}	4.3×10^{-2}	1.6×10^{-15}	6.3×10^{-2}	2.8×10^{-1}	
Coefficients	5.28	2.84	0.19	1.58		0.99 (0.93)
P-value	7.4×10^{-7}	3.7×10^{-1}	1.6×10^{-15}	4.9×10^{-1}		
Coefficients	4.89	4.99	0.19			0.98 (0.93)
P-value	6.7×10^{-7}	1.3×10^{-10}	1.6×10^{-15}			

a) Matsunaga and Ziemann (2010); Yeh and Ziemann (2015)

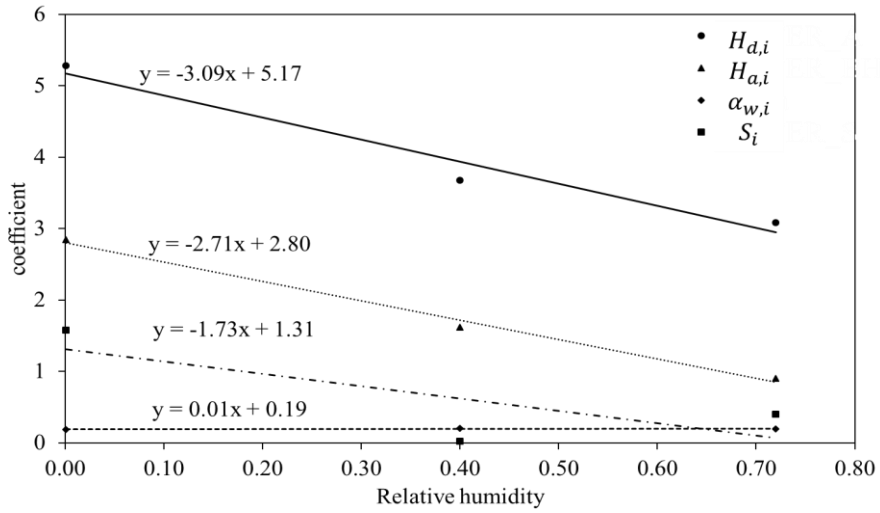

Figure S4. Linear regression results of the coefficient for each physicochemical descriptor correlated to $\ln(\gamma_{w,i})$ under three different humidity levels (RH=0.75, 0.40 for chamber datasets of this study, and RH<0.001 from literature data (Matsunaga and Ziemann, 2010; Yeh and Ziemann, 2015)).

To determine the coefficient for $\alpha_{w,i}$, the backward elimination approach was performed by analyzing the R^2, adjusted R^2, and p-value. The processed statistical outcomes are shown in Table S4.

Table S3. Statistical outcomes of multi-linear regression results through backward elimination

$\alpha_{w,i}$ (R^2=0.75, adj-R^2=0.64)						
Descriptor	$H_{d,i}$	$H_{a,i}$	α_i	S_i	E_i	Intercept
Coefficients	-0.89	-1.06	-0.034	-1.16	0.31	-10.89
P-value	1.1×10^{-3}	1.2×10^{-1}	1.5×10^{-2}	1.0×10^{-3}	1.6×10^{-1}	1.2×10^{-9}
$\alpha_{w,i}$ (R^2=0.69, adj-R^2=0.59)						
Descriptor	$H_{d,i}$	$H_{a,i}$	α_i	S_i	E_i	Intercept
Coefficients	-0.84		-0.018	-1.03	0.39	-11.71
P-value	1.9×10^{-3}		3.1×10^{-2}	2.2×10^{-3}	9.5×10^{-2}	1.6×10^{-13}
$\alpha_{w,i}$ (R^2=0.70, adj-R^2=0.60)						
Descriptor	$H_{d,i}$	$H_{a,i}$	α_i	S_i	E_i	Intercept
Coefficients	-0.92	-1.3	-0.039	-0.98		-10.69
P-value	9.9×10^{-4}	7.4×10^{-2}	6.9×10^{-2}	1.7×10^{-3}		5.3×10^{-10}
$\alpha_{w,i}$ (R^2=0.60, adj-R^2=0.51)						
Descriptor	$H_{d,i}$	$H_{a,i}$	α_i	S_i	E_i	Intercept
Coefficients	-0.87		-0.021	-0.77		-11.68
P-value	2.4×10^{-3}		2.4×10^{-2}	7.2×10^{-3}		7.4×10^{-14}

Section S4. The prediction of $F_{g,i}$ for various compounds with QSAR-based model

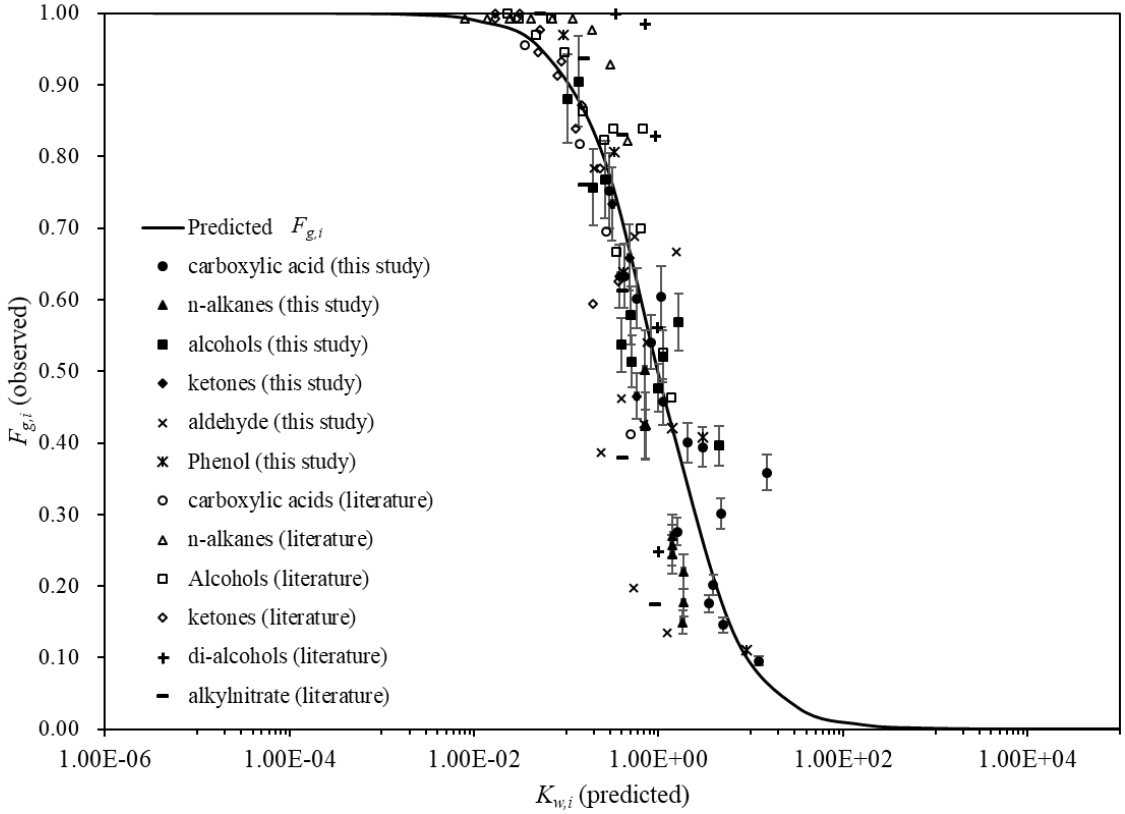

Figure S5. The predicted $F_{g,i}$ (line) and the experimentally observed $F_{g,i}$ (plot) for various SVOCs chamber data sourced from this study under various humidity (RH=0.40, 0.53, 0.75) and the data reported in literatures (Yeh and Ziemann, 2014, 2015; Matsunaga and Ziemann, 2010). The error bar associate with $F_{g,i}$ is estimated using standard deviation of the $C_{g,i}$ measured concentrations of internal standard (7–11%).

Section S5. Calculation of major atmospheric processes' characteristic time

Table S4 summarizes the mathematical equations used to estimate the important atmospheric processes' characteristic time (τ) that can influence SOA growth in chamber studies. Propagation error was calculated for each characteristic time (τ) as ~10 s.

Table S4. Calculation of the τ value of major atmospheric processes in chamber studies.

Process	Important parameters to estimate	Time scales
GWP (τ_{GWP})	$\frac{1}{k_{on,i}+k_{off,i}}$ (S1)	min to h
Gas-particle partitioning (τ_{GP})[a)]	$\tau_{GP} = \frac{1+8\lambda/(\alpha_{p,i}D_p)}{2\pi N_p D_p \lambda v_i}$ (S2) Mean free path of air (λ), mass transfer coefficient ($\alpha_{p,i}$) from gas to particle, number of particles (N_p), particle diameter (D_p), the mean molecular velocity of species i (v_i)	s to min
Gas phase reaction (τ_{OH})	$\tau_{OH} = \frac{1}{k_{OH,i}\times[OH]}$ (S3) $k_{OH,i}$ is reaction rate constant of an organic species with a OH radical in gas phase	min to day
heterogeneous reaction in organic aerosol and inorganic aqueous phase (τ_{or} and τ_{in}, respectively)	$\tau_{or} = \frac{1+K_{or,i}OM_T+K_{in,i}M_{in}}{K_{or,i}M_{or}} \frac{1}{k_{or}C_{T,i}}$ (S4) $\tau_{in} = \frac{1+K_{or,i}OM_T+K_{in,i}M_{in}}{K_{in,i}M_{in}} \frac{1}{k_{in}C_{T,i}}$ (S5) "or" and "in" denote organic phase and inorganic aqueous phase. $K_{or,i}$ and $K_{in,i}$ are the partitioning coefficients of gas/or and gas/in, respectively. OM_T and M_{in} are particulate concentrations (μg m^{-3}) of organic aerosol and inorganic aerosol, respectively. k_{or} and k_{in} are the reaction rate constants of SVOC in or and in phase, respectively.	s to h

a) λ is the mean free path of air (=6.8 μm) and D_p and N_p are assumed to be 100 nm, and 5×10^4 cm^{-3}, respectively (Bowman et al., 1997).

Table S5. The τ values[a] of major atmospheric processes (Table S3) of important oxygenated products sourced from atmospheric oxidation of toluene, isoprene, and α-pinene.

Compound[b] (reactivity[c])	structure (SMILE)	MW (g mol^{-1})	HC[d]	p_L° at 298K[e] (mmHg)	$C_{T,i}$[f] (μg m^{-3})	k_{OH} ($\times 10^{-12}$) (cm^3 molecules^{-1}s^{-1})	k_{or} (L mol^{-1}s^{-1})	k_{in} (L mol^{-1}s^{-1})	τ_{GWP} (s)	τ_{GP} (s)	τ_{OH} (s)	τ_{or} (s)	τ_{in} (s)	Reference
TLEPOXMUC (F)	O=CC1OC1C=CC(=O)C	140.1	Tol	3.84×10^{-4}	1.39	80	9.6	5.7×10^{2}	9248	12	942	19791	126	Im et al. (2014); Beardsley and Jang (2016); Zhou et al. (2019)
CO14O3CHO (F)	O=CCOC(=O)C=O	116.1	Tol	3.15×10^{-1}	0.966	34	9.6	5.7×10^{2}	11639	11	2189	22559	23	
ACCOMECHO (M)	O=CCC(=O)OC(=O)C	130.1	Tol	2.14×10^{-1}	1.09	71	0.12	6.9	6632	12	1062	2611796	5061	
C5CO14OH (S)	CC(=O)C=CC(=O)O	114.1	Tol	3.83×10^{-1}	4.36	54	1.5×10^{-4}	9.1×10^{-3}	3633	11	1384	480033269	1762176	
TLEMUCCO (VF)	O=CC1OC1C(O)C(=O)C(=O)C	172.1	Tol	4.14×10^{-1}	1.68	41	794	4.8×10^{4}	38256	13	1855	0.19	0.0005	
NC4MDCO2H (M)	O=CC(=C(C)C(=O)O)N(=O)=O	159.1	Tol	3.09×10^{-4}	7.94	3.6	0.12	6.9	15125	13	20968	434	0.44	
MALNHYOHCO (S)	O=C1OC(=O)C(O)C1=O	130.1	Tol	8.46×10^{-4}	3.35	5.7	1.5×10^{-4}	9.1×10^{-3}	22886	12	13256	1762075	811	
Glyoxal	O=CC=O	58.0	Tol, Iso	4.19	33.8	9.7	5.0×10^{7}	5.0×10^{9}	335	8	7775	0.02	0.00002	
Iepoxydiol (M)	OCC1OC1(C)CO	118.1	Iso	1.57×10^{-2}	5.64	12	0.12	6.9	11733	11	6491	20798	388	Beardsley and Jang (2016)
Pinic acid (S)	OC(=O)CC1CC(C(=O)O)C1(C)C	186.2	α-p	7.38×10^{-7}	9.76	7.3	1.5×10^{-4}	9.1×10^{-3}	25332	14	10328	32207	21	
Pinonic acid (S)	OC(=O)CC1CC(C(=O)C)C1(C)C	184.2	α-p	3.41×10^{-4}	21.4	6.7	1.5×10^{-4}	9.1×10^{-3}	18516	14	11322	4322	41	
Pinonaldehyde (M)	O=CCC1CC(C(=O)C)C1(C)C	168.2	α-p	6.52×10^{-2}	132	39	0.12	6.9	8131	13	1940	3680	48	

a) For the estimation of τ values, M_{in}= 10 μg m^{-3}, M_{or}=10 μg m^{-3}, and [OH]= 1.33×10^{7} molecules cm^{-3}

b) The names of the structure in toluene products are from MCM products (Master Chemical Mechanism (MCM) version 3.3.1 (Jenkin et al., 2012)).

c) The reactivity scale of SVOC was sourced from the UNIPAR SOA model. The rank of the reactivity scale is as follows: VF (Very Fast)>F (Fast)>M (Medium)>S (Slow)>P (no reaction).

d) Tol, Iso, and α-p denotes toluene, isoprene, and α-pinene, respectively.

e) Calculated through group contribution (Zhao et al., 1999; Stein and Brown, 1994).

f) $C_{T,i}$ is the total concentrations at noon under the low NOx condition (CH (ppbC) /NOx (ppb) >5.5). For the photooxidation of toluene, the initial condition was 130 ppb toluene, 20 ppb NOx (CH (ppbC)/NOx (ppb) = 6.5) on Apr 23, 2014. The initial condition of isoprene oxidation was 500 ppb isoprene, 25 ppb NOx (CH (ppbC)/NOx (ppb) = 20) on Dec 3, 2012. The initial condition of ap oxidation was 170 ppb toluene, 25 ppb NOx (CH (ppbC)/NOx (ppb) = 6.9) on Dec 11, 2010.

References

Barton, A. F. M.: CRC handbook of solubility parameters and other cohesion parameters, 2nd ed., CRC Press, Boca Raton, 739 p. pp., 1991.

Beardsley, R., Jang, M., Ori, B., Im, Y., Delcomyn, C., and Witherspoon, N.: Role of sea salt aerosols in the formation of aromatic secondary organic aerosol: yields and hygroscopic properties, Environmental Chemistry, 10, 167-177, 10.1071/EN13016, 2013.

Beardsley, R., and Jang, M.: Simulating the SOA formation of isoprene from partitioning and aerosol phase reactions in the presence of inorganics, Atmospheric Chemistry and Physics, 16, 5993-6009, 10.5194/acp-16-5993-2016, 2016.

Bowman, F., Odum, J., Seinfeld, J., and Pandis, S.: Mathematical model for gas-particle partitioning of secondary organic aerosols, Atmospheric Environment, 31, 3921-3931, 10.1016/S1352-2310(97)00245-8, 1997.

Fredenslund, A.: Vapor-liquid equilibria using UNIFAC: a group-contribution method, Elsevier, 2012.

Im, Y., Jang, M., and Beardsley, R.: Simulation of aromatic SOA formation using the lumping model integrated with explicit gas-phase kinetic mechanisms and aerosol-phase reactions, Atmospheric Chemistry and Physics, 14, 4013-4027, 10.5194/acp-14-4013-2014, 2014.

Jang, J., Jang, M., Mui, W., Delcomyn, C., Henley, M., and Hearn, J.: Formation of Active Chlorine Oxidants in Saline-Oxone Aerosol, Aerosol Science and Technology, 44, 1018-1026, 10.1080/02786826.2010.507612, 2010.

Jang, M., Kamens, R., Leach, K., and Strommen, M.: A thermodynamic approach using group contribution methods to model the partitioning of semivolatile organic compounds on atmospheric particulate matter, Environmental Science & Technology, 31, 2805-2811, 10.1021/es970014d, 1997.

Jang, M., and Kamens, R.: A thermodynamic approach for modeling partitioning of semivolatile organic compounds on atmospheric particulate matter: Humidity effects, Environmental Science & Technology, 32, 1237-1243, 10.1021/es970773w, 1998.

Jenkin, M., Wyche, K., Evans, C., Carr, T., Monks, P., Alfarra, M., Barley, M., McFiggans, G., Young, J., and Rickard, A.: Development and chamber evaluation of the MCM v3.2 degradation scheme for beta-caryophyllene, Atmospheric Chemistry and Physics, 12, 5275-5308, 10.5194/acp-12-5275-2012, 2012.

Li, J., Jang, M., and Beardsley, R.: Dialkylsulfate formation in sulfuric acid-seeded secondary organic aerosol produced using an outdoor chamber under natural sunlight, Environmental Chemistry, 13, 590-601, 10.1071/EN15129, 2016.

Matsunaga, A., and Ziemann, P.: Gas-Wall Partitioning of Organic Compounds in a Teflon Film Chamber and Potential Effects on Reaction Product and Aerosol Yield Measurements, Aerosol Science and Technology, 44, 881-892, 10.1080/02786826.2010.501044, 2010.

Yeh, G., and Ziemann, P.: Alkyl Nitrate Formation from the Reactions of C-8-C-14 n-Alkanes with OH Radicals in the Presence of NOx: Measured Yields with Essential Corrections for Gas-Wall Partitioning, Journal of Physical Chemistry a, 118, 8147-8157, 10.1021/jp500631v, 2014.

Yeh, G., and Ziemann, P.: Gas-Wall Partitioning of Oxygenated Organic Compounds: Measurements, Structure-Activity Relationships, and Correlation with Gas Chromatographic Retention Factor, Aerosol Science and Technology, 49, 726-737, 10.1080/02786826.2015.1068427, 2015.

Zhong, M., and Jang, M.: Dynamic light absorption of biomass-burning organic carbon photochemically aged under natural sunlight, Atmospheric Chemistry and Physics, 14, 1517-1525, 10.5194/acp-14-1517-2014, 2014.

Zhou, C., Jang, M., and Yu, Z.: Simulation of SOA formation from the photooxidation of monoalkylbenzenes in the presence of aqueous aerosols containing electrolytes under various NO x levels, Atmospheric Chemistry and Physics, 19, 5719-5735, 2019.